applied sciences

MDPI

Article

Optimization of Laser Fired Contact Process for the Formation of an Al-BSF Layer

Jeong Eun Park [1], Won Seok Choi [2] and Donggun Lim [1,2,*]

[1] Department of Electronic Engineering, Korea National University of Transportation, Chungju 27909, Korea; ac1331@naver.com
[2] Department of IT Convergence, Korea National University of Transportation, Chungju 27909, Korea; cws92929@naver.com
* Correspondence: dglim@ut.ac.kr

Abstract: The back-surface field (BSF) layer obtained through the laser fired contact (LFC) process is the key to increasing the efficiency of solar cells. In this paper, we studied the optimization of LFC process parameters—focusing on laser frequency, influence, and speed—to achieve good ohmic contacts, and to reduce the heat-affected zone (HAZ). As frequency increases, interactions between the laser and particles increase, with the particles becoming overly heated. This generates the thermal effect, in which heat is transferred to particles not directly affected by the laser—resulting in the HAZ becoming wider and deeper. Under different laser power conditions, depths of approximately 18 and 8.3 µm were observed at laser speeds of 10 and 100 mm/s, respectively. This analysis of performance variables allowed us to identify those best suited to forming an Al-BSF layer approximately 1.2 µm thick, which resulted in the best LFC procedure while minimizing the HAZ area. HAZ size was minimized at a frequency of 400 kHz, using 5 W laser power, and a laser speed of 100 mm/s, while the best cell characteristics were obtained using a laser pitch of 500 µm and a single laser process.

Keywords: crystalline silicon solar cell; laser fired contact; back surface field; heat affected zone; green nanosecond laser

check for updates

Citation: Park, J.E.; Choi, W.S.; Lim, D. Optimization of Laser Fired Contact Process for the Formation of an Al-BSF Layer. *Appl. Sci.* **2021**, *11*, 2689. https://doi.org/10.3390/app11062689

Academic Editor: Allen M. Barnett

Received: 7 February 2021
Accepted: 15 March 2021
Published: 17 March 2021

1. Introduction

Research and development on new and renewable energy that can replace fossil fuels is underway in various countries. Among renewable energy sources, solar energy is a popular option, as it is the most readily available energy source, and is safe and reliable. Crystalline silicon (c-Si) solar cells currently account for more than 80% of the global solar cell market and have an efficiency of approximately 22% [1]. The goals of the solar cell industry include being able to reduce manufacturing costs (through the value chain of production systems) and to improve efficiency through technology research [2]. Recent research on high-efficiency c-Si solar cells has involved various aspects, such as texturing, doping, antireflection films, materials and structures of the front and rear electrodes, and surface passivation.

The technical development of emitter formation and back field effect aspects are critical for manufacturing high-efficiency c-Si solar cells, and various studies have been actively conducted for this purpose. However, when using the thermal diffusion process in the doping process for emitter formation, it has been difficult to control the doping concentration and junction depth precisely. We have also seen that using the wet method for the texturing process results in there being no structural difference between the front and back surfaces, making it difficult to improve the rear field effect.

Laser-fired contact (LFC) solar cells have several advantages compared to other local contact structures. For example, compared with the photolithography process, the process steps and procedures can be greatly reduced; when compared to the screen-printing process, warping of the wafer during the thin wafer process can be prevented. In older photovoltaic (PV) cells, lasers were mainly used for peeling and wafer cutting after the edge area process, but currently, they are used mainly as part of processes aimed at improving efficiency. Examples include the passivated emitter and rear contact (PERC) processes used to form local back contacts [3,4]. Compared with the cells of the full-area aluminum electrode, a solar cell with a PERC structure that forms a localized contact area can increase efficiency by lowering the recombination rate of electrons and holes. In another example, the laser-doped selective emitter (LDSE) process is a technique used to form a heavily doped region on an electrode formation area, which can improve efficiency by lowering the contact resistance.

Most of these new laser-based concepts for developing c-Si photovoltaic efficiency improvement have been applied to either reduce the thermal load of the device, increase passivation on some interfaces, or improve solar cell Ohmic contacts. In the LFC process, a back surface field (BSF) is formed on the back surface, and a p+ layer is formed on the back surface of the p-type wafer, so that the electrons in the p region move to the back surface, to prevent losses caused by recombination. This can reduce the leakage current, and improve the open-circuit voltage (V_{oc}) and fill factor (FF) [5–7].

The biggest problem in the LFC process has been minimizing the thermal damage between the silicon wafer and Al layer during the laser process. This indicates that while higher efficiency can be obtained by improving the rear electrode structure, the associated thermal damage has to be reduced. In the study reported here, a backside structure was formed using various lasers for the LFC process, and the thermal damage and characteristics applied to the silicon wafer were analyzed, in terms of laser selection and laser process conditions, so as to optimize the LFC associated with p-contact formation.

2. Materials and Methods

In our study, we used c-Si wafers with a thickness of 200 μm and resistivity of 1–3 Ω·cm. The saw-damage removal (SDR) process was performed first, to remove saw damage on the substrate, and then the texturing process—which included anisotropic etching with a mixture of KOH and isopropyl alcohol (IPA)—was performed, to lower wafer reflectivity. This process was performed using a process temperature of 80 °C, and a process time of 30 min. After texturing, wafers with random pyramids were doped with phosphorus, by thermal diffusion in a tube furnace, to form p–n junctions. After doping, the sheet resistance of the emitter layer was approximately 60 Ω·cm.

The front SiNx, as an anti-reflection coating (ARC) layer, was formed by plasma-enhanced chemical vapor deposition (PECVD), the front electrode was formed by screen printing, using Ag paste. Aluminum electrodes were formed on the back side, using an e-beam evaporator, and a firing process was performed, using a laser, to form a local back surface field (LBSF) layer.

A nanosecond (ns) green laser, with a wavelength of 532 nm, was used for the laser process, and the z-axis setting was fixed to avoid differences in the process ability due to laser focus size. The parameters for the ns laser used in this study have been listed in Table 1. To optimize the LFC process, the characteristics of the layer to be processed were analyzed, and the wavelength region of the laser was selected. In this experiment, the LFC process was performed using varied laser parameters; the laser pitch for the LFC pattern varied between 250–1000 μm.

Table 1. Parameters for the laser used in the process.

Laser Parameters	Conditions
Laser type	Nanosecond green laser
Beam mode	Pulsed mode
Focal spot diameter	3.5 mm at a laser power of 8.6 W
Focal spot position (z-axis)	0 um
Pulse frequency range	10–600 kHz
Laser moving system	XYZ system
Output power range	0.1–10 W
Wavelength	532 nm

After laser processing, Si surface morphologies were analyzed, using a Hitachi S-4300 scanning electron microscope (SEM), with an operating voltage of 25 kV, and quantum efficiencies were measured, using a McScience K3100 ATX spectral incident photon-to-current conversion efficiency (IPCE) measurement system, under AM 1.5 G illumination, and 100 mW/cm^2 power density.

3. Results

We worked with an ns green laser when applying P-contact formation technology to the back of the silicon wafer through the LFC process. When the laser is used this way, a heat-affected zone (HAZ) inevitably occurs, as when the laser beam is irradiated to the metal layer on the silicon solar cell, all its energy is absorbed, apart from the reflected part. The HAZ is an area of the base material where the material does not melt when exposed to high temperatures, although its microstructure and mechanical properties are affected by both the heat generated during the laser and the sequential cooling processes. The HAZ can have undesirable effects, such as surface cracks and distortion, and ultimately causes wafer damage, degrading cell characteristics. Accordingly, it is necessary to select appropriate laser parameters to minimize the HAZ, and so, in this study, we studied ns laser process optimization so as to minimize the HAZ formed during p-contact formation.

In a solar cell characterized by the LFC structure, it is essential to form a Si/Al alloy, by instantaneously melting Si and Al under the correct laser conditions. During this, if the energy of the laser is excessive, the Al layer evaporates, while if the energy is too weak, only the surface of the Al melts, and proper alloy formation will not occur. In this study, laser conditions were analyzed structurally and electrically, in terms of the frequency, power, and speed of the ns laser, when applied to LFC structure solar cell fabrication.

First, we analyzed the structure of the p-contact processing region, in relation to ns laser frequency. After fixing the laser power at 7 W and a speed of 100 mm/s, the frequency was varied between 300–600 kHz. To assist our analysis of the HAZ generated during the laser process, scanning electron microscope (SEM) imagery of the affected surfaces and cross-sections were obtained, as shown in Figure 1.

In Figure 1, it can be seen that, at 500 kHz or higher, laser damage rapidly increases. This is because, as the frequency increases, the number of processes between the laser and particles increases; the particles then become excessively heated, which transfers heat to particles that are not directly affected by the laser. This indirect thermal effect increases laser damage around the processed laser track.

The SEM imagery in Figure 2 shows that the laser track width increased as the frequency increased from 300 to 600 kHz. For frequencies ≤400 kHz, the damage extended over an area <3 μm in diameter. The associated cross-sectional imagery for conditions of 300 and 400 kHz, showed that the processing had reached depths of approximately 5.2 and 9.2 μm, respectively. However, the 300 kHz image showed that the energy density for forming the Al-BSF layer was so low that only the surface had been processed, making such a frequency unsuitable for p-contact formation. Thus, a 400 kHz process was identified as the most suitable for LFC structure solar cell fabrication. In order to optimize the formation of the BSF layer in a manner in which silicon wafer thermal damage at the HAZ was minimal, the frequency was fixed at 400 kHz, and the experiment on the effect of varying laser power was allowed to proceed.

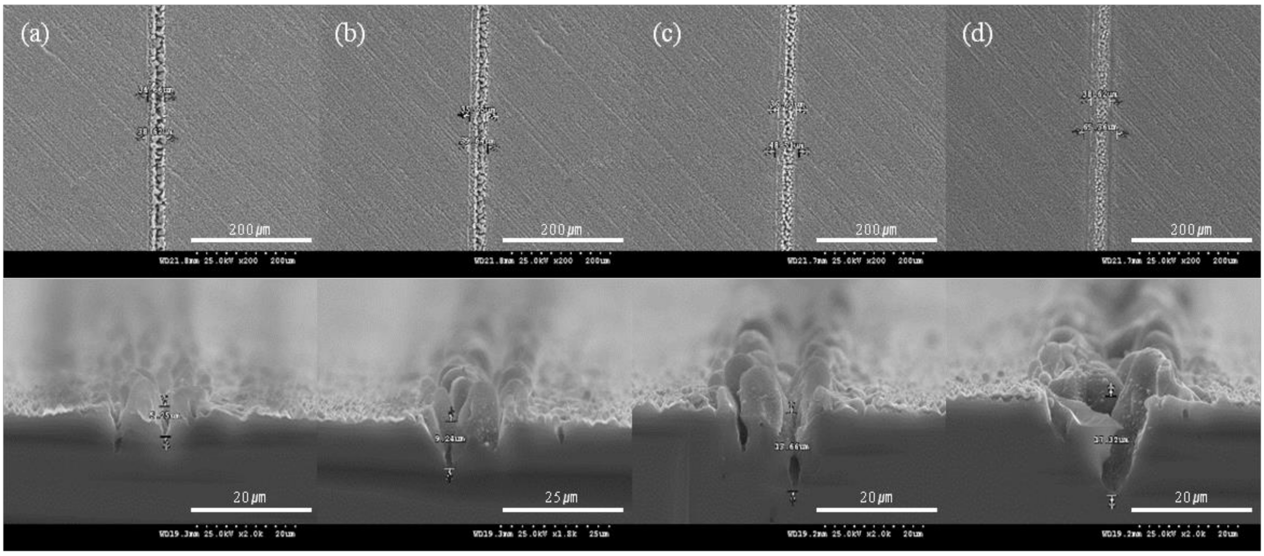

Figure 1. SEM imagery of wafer surfaces and cross-sections after ns laser processing, using various laser frequencies: (**a**) 300 kHz; (**b**) 400 kHz; (**c**) 500 kHz; (**d**) 600 kHz.

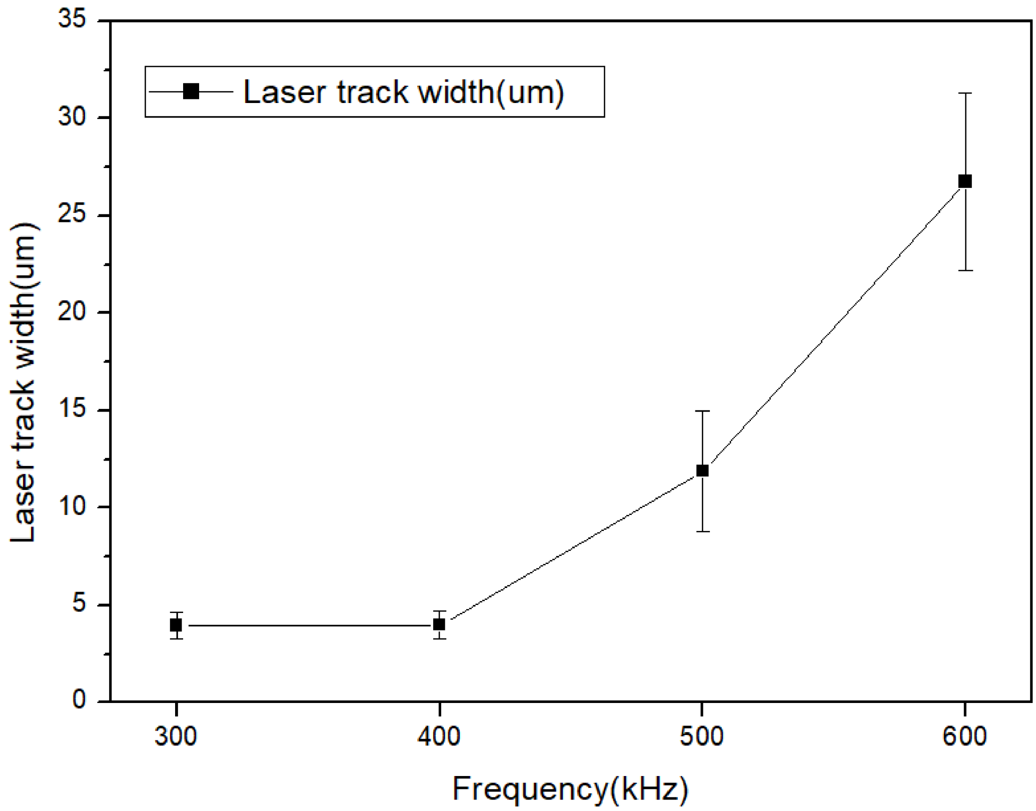

Figure 2. Graph of laser track width vs. laser frequency.

SEM imagery of the surfaces and cross-sections after the application of different laser powers (after fixing the laser speed at 100 mm/s and the frequency to 400 kHz), can be seen in Figure 3. It can be seen that 4 W was not suitable for the LFC process, as the energy density was too low for p-contact formation, and the process was not performed smoothly. The process depths of approximately 8.31 and 8.33 μm were achieved when using conditions of 5 and 6 W, respectively, creating respective HAZ diameters of approximately 8.69 and 14.25 μm, respectively, which were suitable conditions for p-contact formation. At 7 W, the solidification phenomenon—which occurs due to excess heating and melting—was seen to occur during the process. It was also apparent at this power that the dimensional precision of the processed portion was reduced, and that the process had become difficult to control. While the depth was approximately 8.5 μm under the power of 7 W, it was simply not suitable due to the excessive melting and the size of the HAZ created during p-contact formation. Based on these findings, laser powers of 5 and 6 W were used in the next experimental phase of the optimization process, which involved changing the laser speed.

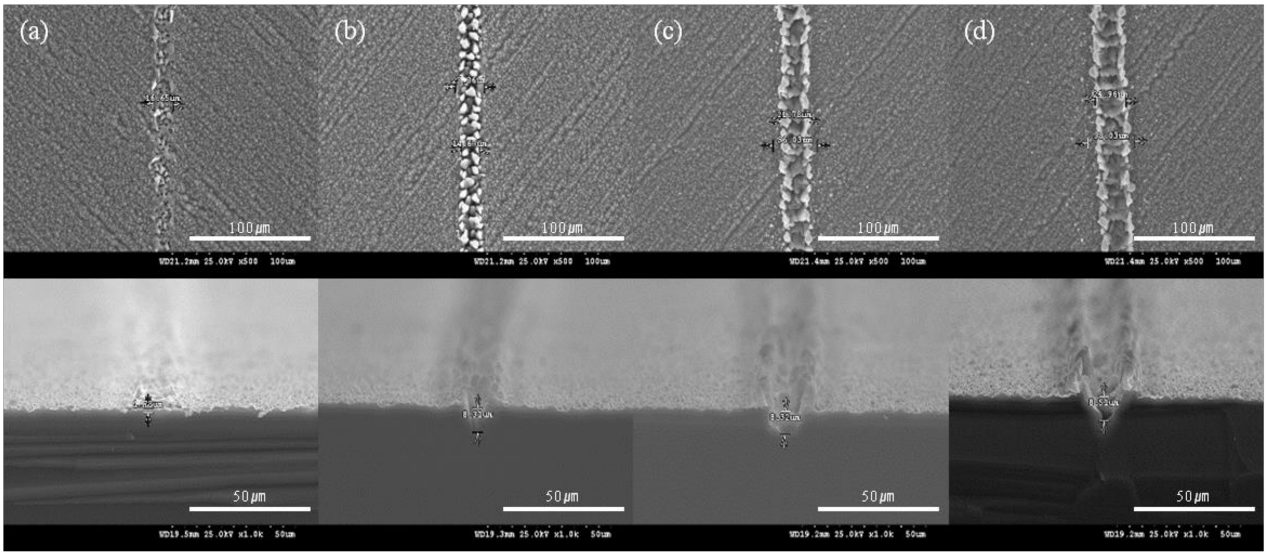

Figure 3. SEM imagery of wafer surfaces and cross-sections according to varied laser power, under conditions of 100 mm/s laser speed, and a frequency of 400 kHz: (**a**) 4 W; (**b**) 5 W; (**c**) 6 W; (**d**) 7 W.

Figures 4 and 5 include SEM imagery of wafers processed at different laser speeds, with laser powers of 5 and 6 W, while Figure 6 shows the laser track widths using the same 5 and 6 W laser powers. In these experiments (using 5 and 6 W laser power), the line widths were different from the expected values at these laser speeds. The laser track width was expected to decrease as the laser speed increased, however, it increased at a laser speed ≥500 mm/s. This was related to the formation of large molten layers caused by the excess energy near the laser processing area. That is, when the laser speed was low, local heat propagation lasted longer, and thus the sample surface temperature increased, owing to the higher laser beam residence time. The heat-affected region increased, and a phase change from the solid-state was seen, reflecting the increased depth of the heat-affected region during the cooling period.

At lower speeds, the laser track width increased accordingly, as the laser speed decreased. At higher laser speeds, sample heat propagation was short-lived, which resulted in less sample surface damage and a decreased laser track width.

The case where experimental outcomes differed from the expected values saw the total laser line width the same as the previous condition, but molten solids remained on the surface, due to the thermal effect. Through this result, it was confirmed that when the process was conducted at laser speeds ≥500 mm/s, the process failed, because the energy density applied per unit area was too low due to the combination of high speed and low power density.

These outcomes revealed that the suitable structural characteristics for p-contact formation—which occurred when the melting and thermal damage such as HAZ were minimized—were observed under conditions of 5 W laser power, a speed of 100 mm/s, and a frequency of 400 kHz. To ensure that conditions for the BSF layer were optimized, layers were structurally analyzed using SEM imaging for each laser speed, at the 5 W power setting.

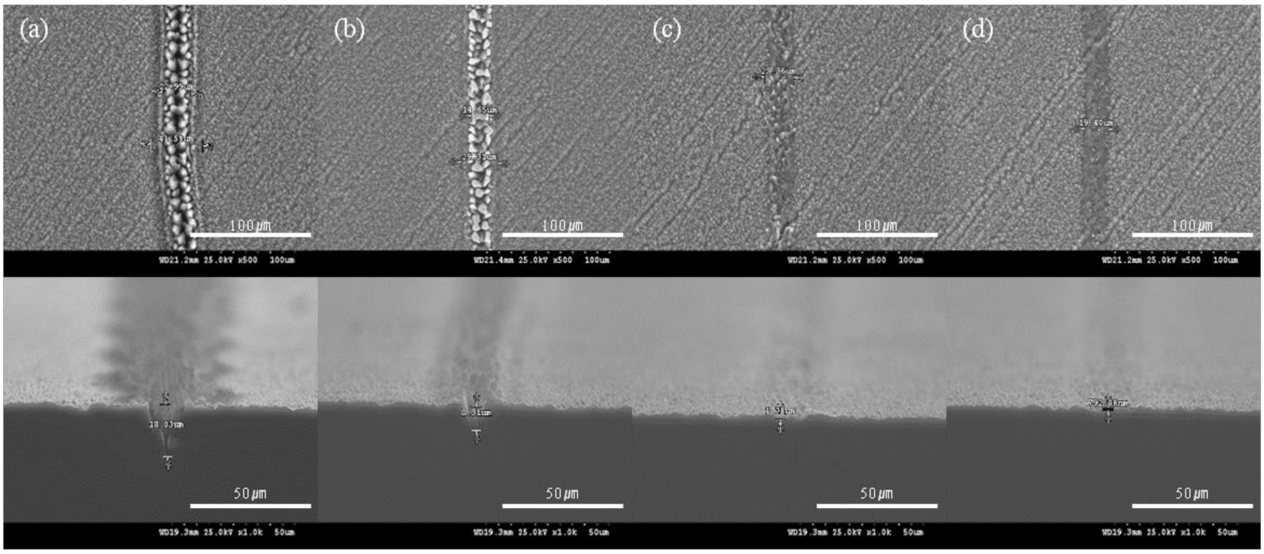

Figure 4. SEM imagery of wafer surfaces and cross-sections in response to varied laser speeds, at 5 W laser power: (**a**) 10 mm/s; (**b**) 100 mm/s; (**c**) 500 mm/s; (**d**) 1000 mm/s.

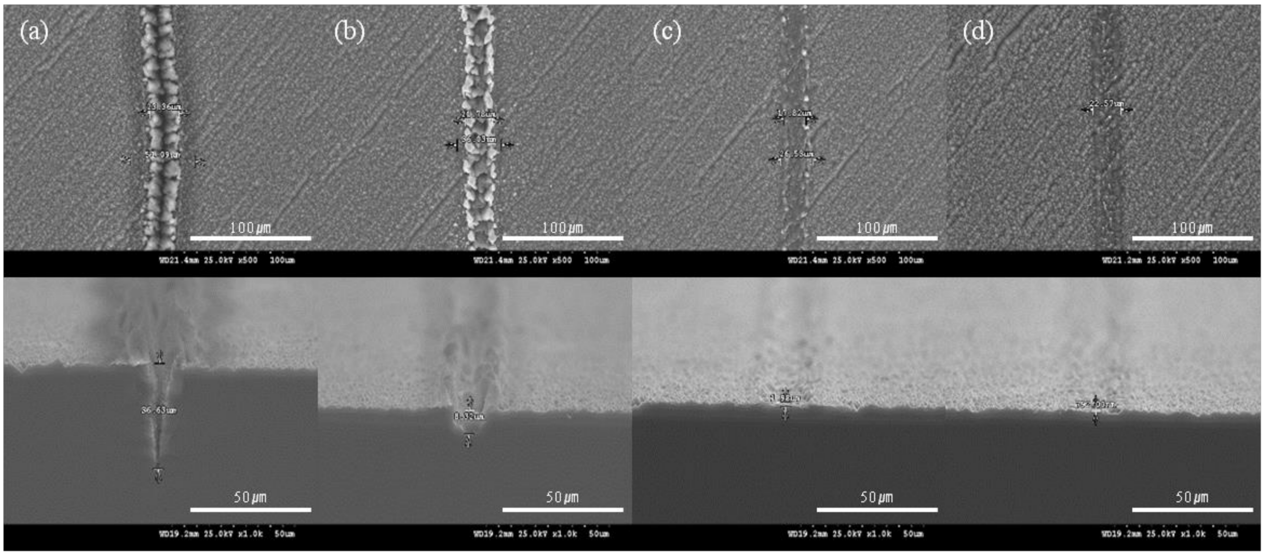

Figure 5. SEM imagery of wafer surfaces and cross-sections in response to varied laser speeds, at 6 W laser power: (**a**) 10 mm/s; (**b**) 100 mm/s; (**c**) 500 mm/s; (**d**) 1000 mm/s.

Figure 7 shows the SEM imagery of BSF layers prepared using laser speeds from 10–500 mm/s. In the case of the Al-BSF layer, it is critical to collect the minority electrons in the solar cell of the p-type substrate, as the BSF layer, the p+ region at the back, pushes electrons to the opposite side, thus facilitating the collection of holes due to the field effect. This reduces the probability of electron/hole recombination, and increases the number of electrons collected, resulting in improved electrical properties—hence, the thickness of the BSF layer is important.

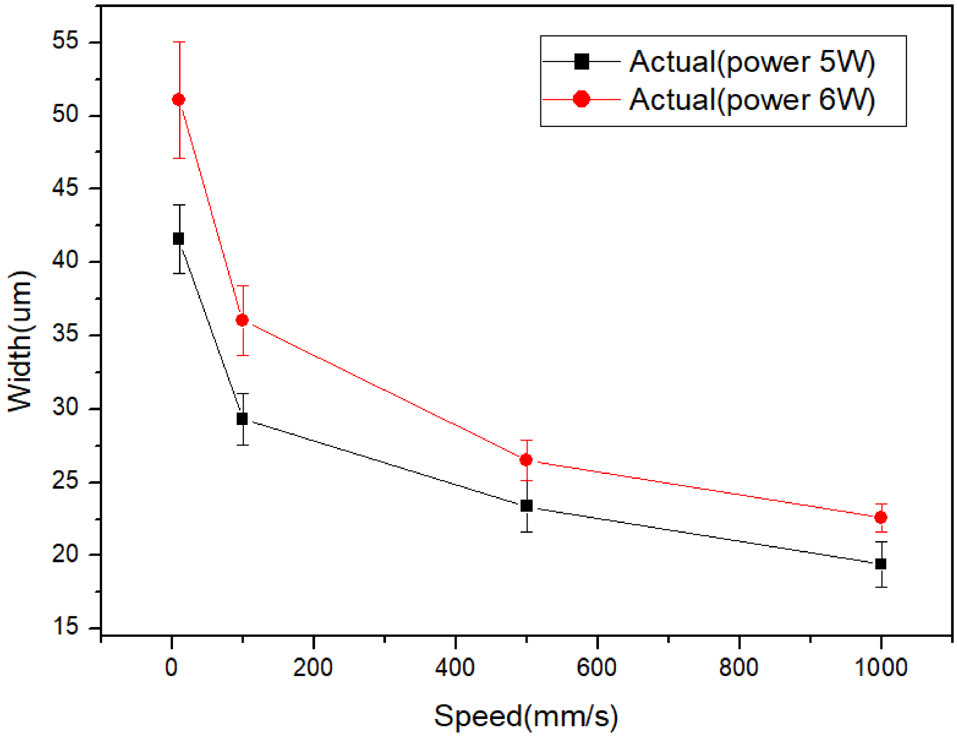

Figure 6. Laser track widths for 5 and 6 W laser power settings.

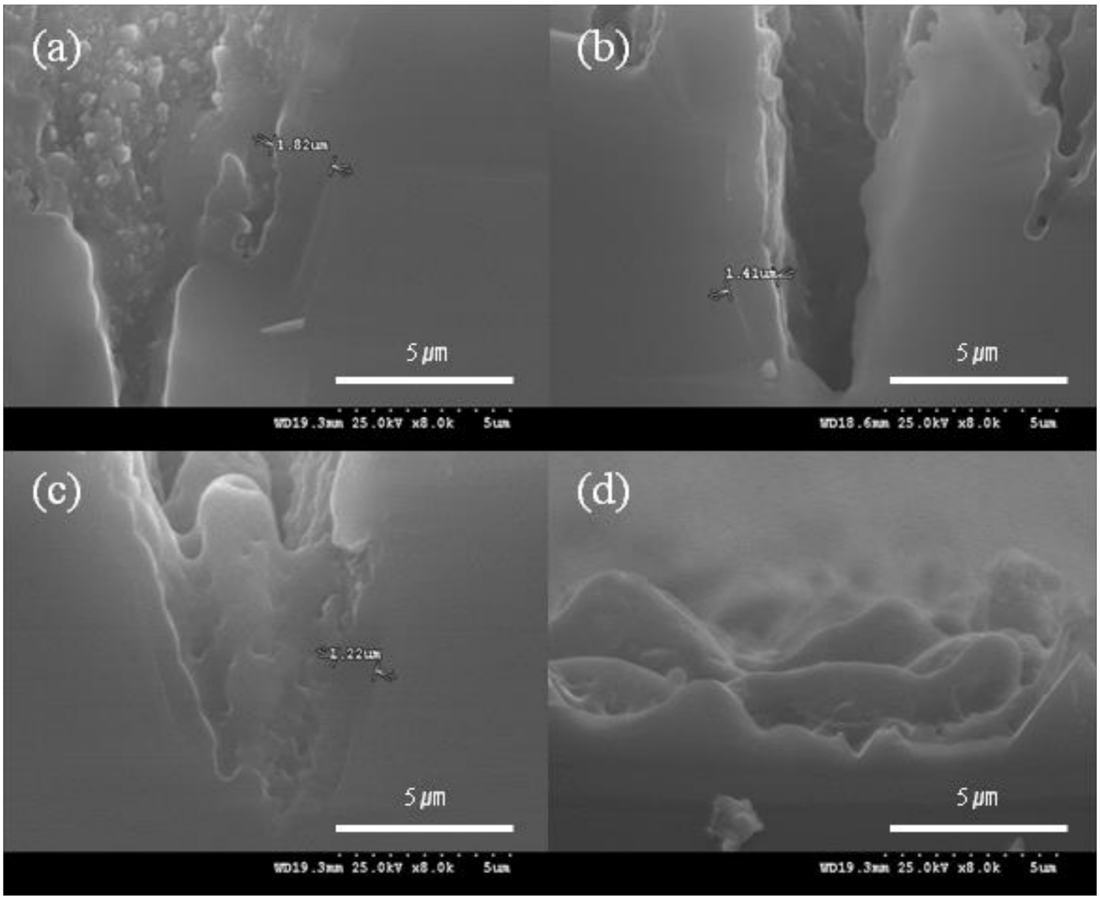

Figure 7. SEM image of the Al-BSF layer in relation to operating laser speed: (**a**) 10 mm/s; (**b**) 50 mm/s; (**c**) 100 mm/s; (**d**) 500 mm/s.

It can be seen in Figure 7 that the Al-BSF layer was not observed at a laser speed of ≥500 mm/s. In this case, sufficient heat was not applied to the Al layer, due to the relatively low energy, and only the surface of the Al layer was processed to confirm that the alloy was not formed. However, the Al-BSF layer was ~1.82 µm at 10 mm/s laser speed, ~1.41 µm at 50 mm/s, and ~1.22 µm at 100 mm/s.

Figure 8 shows the thickness and SEM image of the Al-BSF layer according to the laser speed with a fixed laser power of 5 W. As shown in Figure 8, the thickness of the Al-BSF layer gradually decreased as the laser speed increased, and a thick Al-BSF layer was observed at laser speeds of 10 mm/s and 50 mm/s. At lower laser speed, the thermal energy absorbed by the metal electrode material increased, making it more affected by the laser process. When the laser speed increased, the residence time of the laser beam in the process area of the cell was less, and the interaction time between the materials of the metal electrodes and laser was also reduced. This confirmed that the thickness of the Al-BSF layer decreased at higher laser speeds because the energy required for BSF layer formation had not been transferred sufficiently to the process area.

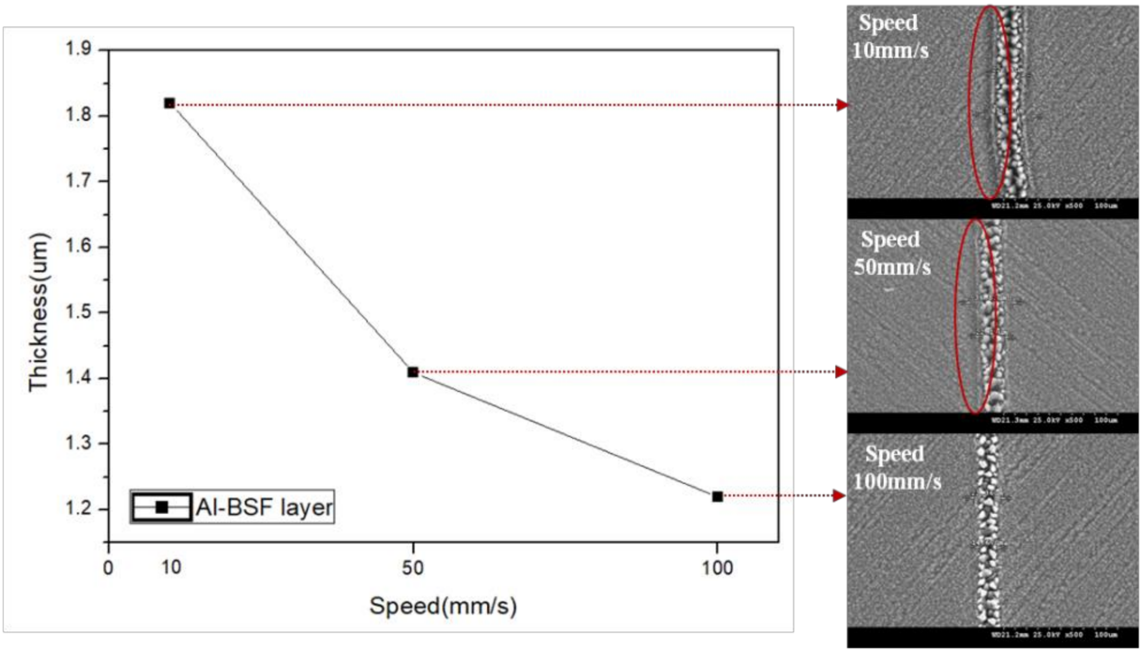

Figure 8. The thickness and SEM image of the Al-BSF layers created using various laser speeds, with laser power fixed at 5 W.

When analyzing the surface image, it can be seen that the silicon wafer has the greatest damage due to the HAZ on both sides of the laser track. However, the Al-BSF layer of adequate thickness was formed in compliance with a laser speed of 100 mm/s, in which case, SEM imagery confirmed that the associated thermal damage was minimal.

Based on these results, the laser characteristics optimized for LFC—5 W laser power, laser speed of 100 mm/s, and frequency of 400 kHz—were fixed, and electrical characteristics were then analyzed. To fabricate a solar cell with an LFC structure, electrical analyses were conducted by varying the laser pitch through 250, 500, 750, and 1000 µm, and conducting the laser processes between one and three times.

Figure 9 shows the external quantum efficiency (EQE) graph measured after fabricating the solar cell using one, three, and five treatment repeat numbers, and four different laser pitches. If the pitch of the laser was too wide, the contact area of the electrode was narrow, causing less BSF layer to be formed. In contrast, with too narrow a pitch of the laser, an overlapping portion may result, because of the thermal effect of the laser, and efficiency may be reduced. Figure 9a shows the EQE graph for solar cells fabricated against the number of processing repeats and confirms that the EQE decreased as the number of laser process repeats increased. This reduction may be caused by laser-induced damage, which generates recombination. In Figure 9b, the quantum efficiency values for all conditions were similar at short wavelengths, while the efficiency at a pitch of 500 µm was relatively high, at long wavelengths, leading to excellent light generation carriers.

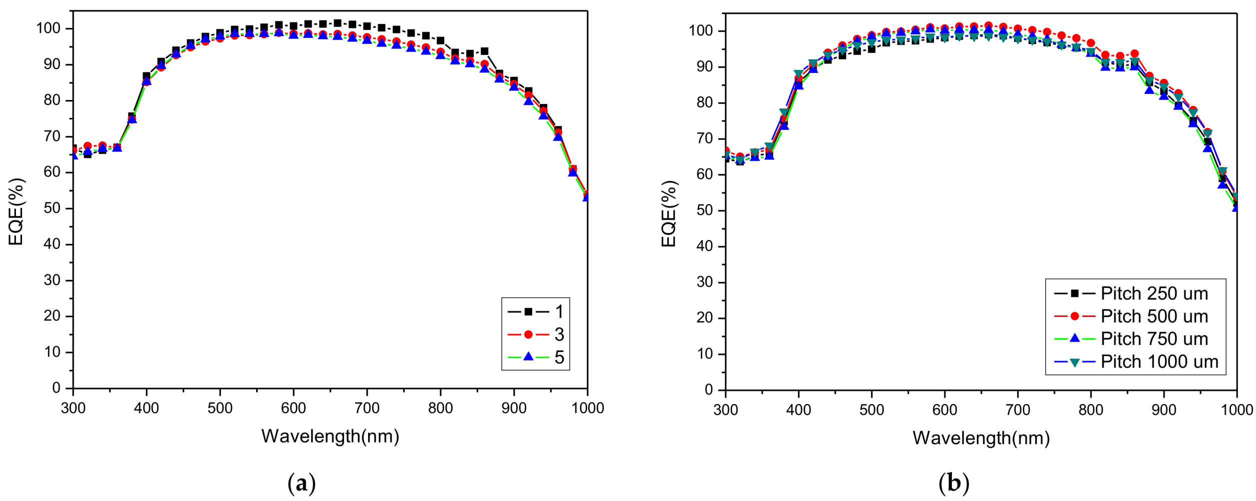

Figure 9. Quantum efficiency graph measured after fabricating the solar cell using: (**a**) one, three, and five treatment repeat numbers; and (**b**) four different laser pitches.

From this test series, we were able to conclude that the best EQE was obtained using a laser pitch of 500 µm, and a single process (without the need for any repeats).

4. Conclusions

In this work, we studied laser frequencies, power, and speed, to optimize the LFC development process. The HAZ, which inevitably occurs as a result of the laser process, aggravates cell characteristics, and so the LFC process must be performed using a laser process optimized to create a minimal HAZ. Nanosecond green lasers were used to obtain the thickest BSF layer through the LFC process, and the testing described herein showed that the best LFC procedure was achieved with a 1.2 µm-thick Al-BSF layer. The HAZ size was minimized at a frequency of 400 kHz, using 5 W laser power, and a laser speed of 100 mm/s. For their electrical analysis, LFC solar cells were fabricated by adjusting the laser pitch and the number of application repeats. The resulting EQE analysis showed that the best cell characteristics were obtained using a laser pitch of 500 µm and three times of laser process. Overall, the experimental results allowed us to conclude that the LFC technology was appropriate for use in improving cell characteristics.

Author Contributions: J.E.P. was the main author, carried out the experiments, and analyzed the data. W.S.C. reviewed and analyzed the data and formatting. D.L. conceived the ideas of the analyzed results. All authors participated in discussing the results, reviewing the manuscript, and providing input for editing. All authors have read and agreed to the published version of the manuscript.

Funding: This work was supported by the Korea Electric Power Corporation (Grant number: R17XA05-1), the Korea Institute of Energy Technology Evaluation and Planning (KETEP), and the Ministry of Trade, Industry and Energy (MOTIE) of the Republic of Korea (Grant number: 20193020010650).

Institutional Review Board Statement: Not applicable.

Informed Consent Statement: Not applicable.

Data Availability Statement: Not applicable.

Conflicts of Interest: The authors declare no conflict of interest.

References

1. Höger, I.; Schaper, M.; Mette, A.; Lee, B.G.; Fertig, F.; Lantzsch, R.; Peters, S.; Eidner, A.; Duncker, K.; Bartzsch, M.; et al. Boosting module power by advanced interconnection and p-type Cz silicon solar cell efficiencies exceeding 22% in mass production. *AIP Conf. Proc.* **2018**, *1999*, 110003-1–110003-6.
2. Hallama, B.; Urueña, A.; Russell, R.; Aleman, M.; Abbott, M.; Dang, C.; Wenham, S.; Tous, L.; Poortmans, J. Efficiency enhancement of i-PERC solar cells by implementation of a laser-doped selective emitter. *Sol. Energy Mater. Sol. Cells* **2015**, *134*, 89–98. [CrossRef]
3. Ebser, J.; Sommer, D.; Fritz, S.; Schiele, Y.; Hahn, G.; Terheiden, B. p+-doping analysis of laser-fired contacts for silicon solar cells by Kelvin probe force microscopy. *J. Appl. Phys.* **2016**, *119*, 105707. [CrossRef]
4. Ye, F.; Li, Y.; Jia, X.; Gu, H.; Wang, X.; Ding, J.; Yuan, N.; Feng, Z. Optimization of phosphorus dopant profile of industrial p-type mono PERC solar cells. *Sol. Energy Mater. Sol. Cells* **2019**, *190*, 30–36. [CrossRef]
5. Roige, A.; Alvarez, J.; Kleider, J.-P.; Martin, I.; Alcubilla, R.; Vega, L.F. Microscale spatially resolved characterization of highly doped regions in laser-fired contacts for high-efficiency crystalline Si solar cells. *IEEE J. Photovolt.* **2015**, *5*, 545–551. [CrossRef]
6. He, J.; Hegedus, S.; Das, U.; Shu, Z.; Bennett, M.; Zhange, L.; Birkmire, R. Laser-fired contact for n-type crystalline Si solar cells. *Prog. Photovolt. Res. Appl.* **2015**, *23*, 1091–1099. [CrossRef]
7. Park, C.; Choi, G.; Balaji, N.; Ju, M.; Lee, Y.; Lee, H.; Yi, J. Analysis of laser injection conditions and electrical properties in local BSF for laser-fired contact c-Si solar cell applications. *J. Nanosci. Nanotechnol.* **2018**, *18*, 5013–5019. [CrossRef] [PubMed]